Integrative and Comparative Biology, volume 51, number 1, pp. 142–150
doi:10.1093/icb/icr051

SYMPOSIUM

Effect of Flexural and Torsional Wing Flexibility on Lift Generation in Hoverfly Flight

Hiroto Tanaka,[1,*,†] John P. Whitney[*] and Robert J. Wood[*,†]

[*]School of Engineering and Applied Sciences, Harvard University, 60 Oxford Street, Cambridge, MA 02138, USA; [†]Wyss Institute for Biologically Inspired Engineering at Harvard University, 60 Oxford Street, Cambridge, MA 02138, USA

From the symposium "Bioinspiration: Applying Mechanical Design to Experimental Biology" presented at the annual meeting of the Society for Integrative and Comparative Biology, January 3–7, 2011, at Salt Lake City, Utah.

[1]E-mail: rjwood@eecs.harvard.edu

Synopsis The effect of wing flexibility in hoverflies was investigated using an at-scale mechanical model. Unlike dynamically-scaled models, an at-scale model can include all phenomena related to motion and deformation of the wing during flapping. For this purpose, an at-scale polymer wing mimicking a hoverfly was fabricated using a custom micromolding process. The wing has venation and corrugation profiles which mimic those of a hoverfly wing and the measured flexural stiffness of the artificial wing is comparable to that of the natural wing. To emulate the torsional flexibility at the wing-body joint, a discrete flexure hinge was created. A range of flexure stiffnesses was chosen to match the torsional stiffness of pronation and supination in a hoverfly wing. The polymer wing was compared with a rigid, flat, carbon-fiber wing using a flapping mechanism driven by a piezoelectric actuator. Both wings exhibited passive rotation around the wing hinge; however, these rotations were reduced in the case of the compliant polymer wing due to chordwise deformations during flapping which caused a reduced effective angle of attack. Maximum lift was achieved when the stiffness of the hinge was similar to that of a hoverfly in both wing cases and the magnitude of measured lift is sufficient for hovering; the maximum lift achieved by the single polymer and carbon-fiber wings was 5.9×10^2 μN and 6.9×10^2 μN, respectively. These results suggest that hoverflies could exploit intrinsic compliances to generate desired motions of the wing and that, for the same flapping motions, a rigid wing could be more suitable for producing large lift.

Introduction

Hoverflies are well known for their remarkable flight capabilities including hovering and agile manoeuvres (Ellington 1984b; Brodsky 1994; Fry 2003). Hence, this species is attractive not only to biologists but also to aerodynamicists and engineers who aim to build small flying robots inspired by biological designs (e.g., Wood 2008). Unlike conventional fixed-wing aircraft, a hoverflies' wings are flexible which results in nontrivial deformations during flapping flight (Ellington 1984b; Ennos 1988b; Walker et al. 2009). Although wing flexibility presumably has several benefits for flapping-wing flight such as minimal inertia due to reduced material in the wing and the ability to passively pronate and supinate to reduce the angle of attack, the effects on the flow structure around the wings and the resulting performance is still unclear.

Wing flexibility can be structurally divided into two parts: flexural compliance of the wing surface (both in the spanwise and chordwise directions) and torsional flexibility at the joint connecting the wing and the body. To highlight the importance of wing compliance, the deformation of the wing during flapping depends entirely upon the wing structure since insect wings do not contain muscles that actively change the wing shape. Wings of most flying insects, including hoverflies, consist of tubular veins supporting thin membranes (reviewed by Brodsky 1994; Wootton 1992). Combes and Daniel (2003a) measured the flexural stiffness of various insects wings and found that spanwise flexural stiffness was 1–2 orders of magnitude larger than chordwise flexural stiffness. They also showed that the stiffness changed as a function of the vein stiffness

Advanced Access publication May 27, 2011

using a finite-element model analysis. Actual deformation of the wing of a free-flying hoverfly, *Eristalis tenax*, was recently measured in detail with multiple high-speed video cameras by Walker et al. (2009) showing that the wing surface twists and generates cambered profiles during flight. The torsional wing stiffness of *E. tenax* was measured by Ennos (1988a). This study showed that stiffness in pronation was larger than that in supination. However, measurements of the torsional angle at the base of the wing during free flight are scarce. It is also unknown whether the rotation of the joint is actively caused by the direct flight muscles or passively by joint flexibility, or both.

For a parametric study of the aerodynamics of hovering flight, a dynamically-scaled flapping mechanism with a rigid flat wing was previously used (Dickinson et al. 1999; Birch and Dickinson 2001). Using mechanical models instead of live insects, precise control of wing kinematics and high repeatability were achieved, revealing various unsteady features of the aerodynamics of hovering insects (reviewed by Sane 2003). Recently, dynamically-scaled models recreated the flexibility as well as the kinematics of insect wings to some extent. Ishihara et al. (2009) used a wing model with a plate spring at the rigid leading edge and demonstrated that appropriate torsional flexibility maximized the mean lift coefficient of a crane fly. Zhao et al. (2010) used a wing model consisting of a rigid leading edge and a flexible plastic plate, and showed that the lift coefficient can be increased by the surface flexibility when the angle of attack of the wing was $>50^\circ$ at a Reynolds number of 2000.

Dynamically-scaled models, however, are unable to recreate passive deformation of the wing caused by the combined inertial and aerodynamic forces experienced during flight. Inertia of the wing is thought to play an important role in deformation of the wings of flying insects (Ennos 1988b; Combes and Daniel 2003b). To model the ratio of the inertia of a natural wing to fluid inertial force which can be represented by a mass density ratio of the wing material to fluid (not just the ratio of fluid dynamic pressure to fluid viscous force which can be represented by Reynolds number), using a large dynamically-scaled model would require a material with an unachievably high density (Ishihara et al. 2009). For example, Ishihara's dynamically-scaled model would require a density of $>140\,\mathrm{g\,cm^{-3}}$ for a wing material in order to dynamically scale the density ratio of the wing to the fluid, which is 100 times more dense than the wing material (polyethylene terephthalate) used in the model. For comparison, the densest element, Osmium, has a density of only $22.59\,\mathrm{g\,cm^{-3}}$. Therefore, the effect of wing inertia in a large-scale model is much smaller than that in real insects.

At-scale models operating in air have the potential to simulate the aerodynamic phenomena of compliant flapping wings since the structure, inertia, operating frequency, and trajectories are similar to those of insects in free flight. A hoverfly-sized mechanical robot with flapping wings has been realized using meso-scale manufacturing techniques and piezoelectric actuation (Wood 2008; Whitney and Wood 2010). This device flaps at greater than 100 Hz at a flapping amplitude of 100° and generates lift greater than body weight. A fabrication method for insect-sized flexible wings was also introduced by Tanaka and Wood (2010). These wings, made of a flexible polymer, have venation and corrugated profiles similar to those of a hoverfly (Fig. 1).

In this article, we explore the effect of flexural and torsional flexibility of a hoverfly wing on lift generation by actuating compliant and rigid at-scale wings with trajectories appropriate to hoverfly flight while measuring the resulting lift force. The compliant wing was created to match the morphology of a hoverfly wing using the process described in 'At-scale model of a hoverfly wing' section. This wing matches shape and surface features and stiffness of a natural hoverfly wing. A flexure hinge (the 'wing hinge') at the interface between the wing and thorax was used to enable passive wing rotation and its stiffness was tuned to the measured torsional stiffness of a hoverfly wing. A rigid carbon-fiber (CF) reinforced wing was also fabricated for comparison. Using these at-scale models, we examined our hypothesis that enough lift for hovering can be achieved with passively rotating wing in hoverflies and studied the lift generated by both wings as the wing hinge stiffness was altered. Detailed fabrication methods and experimental results are described in the following sections.

Materials and Methods

At-scale model of a hoverfly wing

Corrugation profiles have been documented for a hoverfly (Rees 1975) as well as a dragonfly (Okamoto et al. 1996; Jongerius and Lentink 2010). Figure 1 illustrates the venation and corrugation profiles of *E. tenax* captured by a photograph and an X-ray CT, respectively. Design of our at-scale model is shown in Fig. 2A and B. The venation and outline were the same as those of *E. tenax*, and the corrugated surface was designed with 3D CAD based on

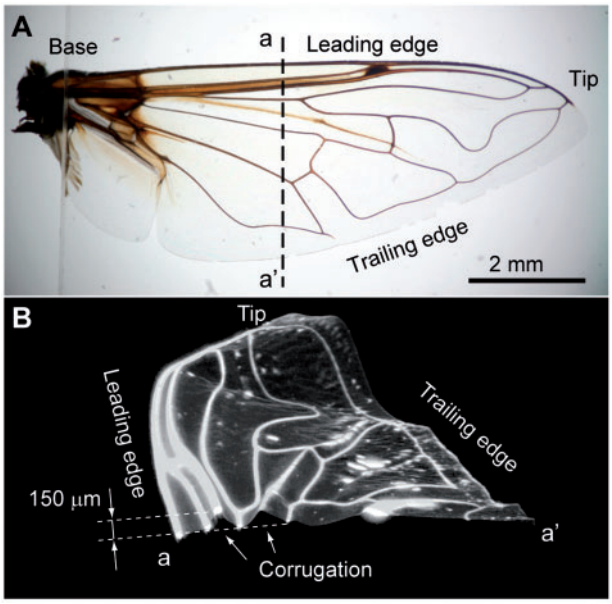

Fig. 1. (**A**) Venation of a right wing of a hoverfly, *Eristalis tenax*. (**B**) X-ray CT image of a corrugated cross-section of a right wing of *Eristalis tenax*.

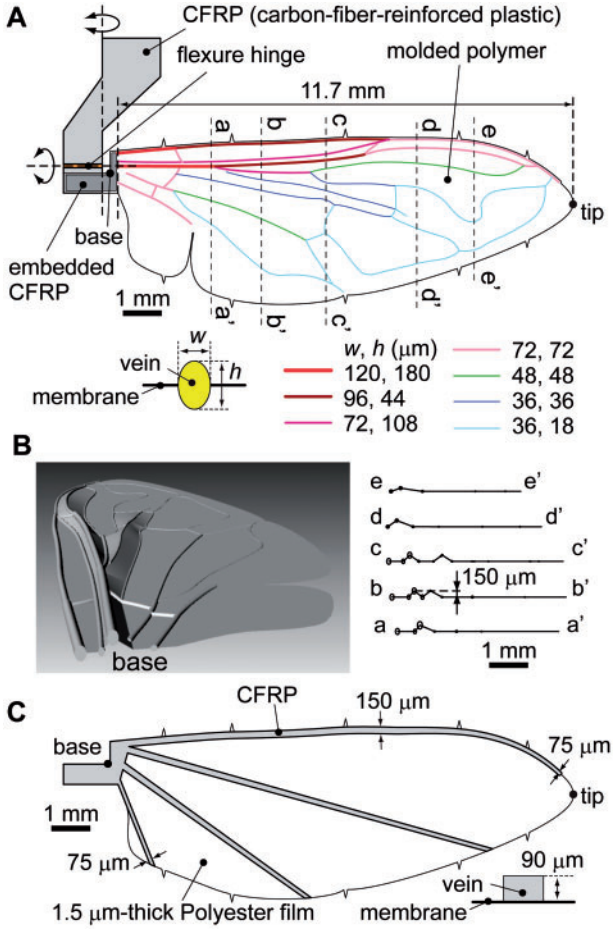

Fig. 2. (**A**) A flexure hinge and venation of a polymer corrugated wing. The thickness of the wing membrane was ~10 μm. A L-shape CFRP (Carbon fiber reinforced polymer) plate was embedded at the wing base to reinforce the connection with the wing hinge. (**B**) Perspective view of the corrugated surface profile created with a 3D CAD software (left) and the cross sections of the wing (right). (**C**) Design of a flat carbon fiber reinforced wing.

the X-ray CT scans. The cross-sectional shape of the artificial veins is a solid ellipse while the natural wing has tubular veins. This is due to the limitation of the fabrication method described below. The width and height of the artificial veins ranges from 36 to 120 μm and 18 to 180 μm, respectively (Fig. 2A). Triangular features at the outline of the wing were used as registration marks for motion tracking. The thickness of the membrane was <10 μm. The corrugation of the artificial wing runs from the wing base to the tip branching in the middle (Fig. 2B) with a maximum height of 150 μm. These design values were chosen to achieve a stiffness similar to that of the natural wing (using the measurement process described below) through multiple revisions. Although the corrugations presumably affect the flexibility of the wing surface and its deformation during the flight, the actual effect of the wing stiffness on aerodynamic performance during flapping is still unclear.

The at-scale corrugated wing was created by molding a thermosetting resin with a pair of micromolds: a bottom silicon mold and a top PDMS (polydimethylsiloxane) mold (Fig. 3). The 3D shapes of the solid veins and membrane of the corrugated wing were simultaneously formed by a single molding process. Complex 3D profiles of the molds for the veins and corrugations were realized by laser-scanning ablation with a pulsed DPSS (diode-pumped solid state) UV laser. The mold surface was etched layer-by-layer with average step height of 3 μm, resulting in arbitrary 3D shapes. The PDMS mold was created by casting PDMS resin on another positive silicon mold made by the laser ablation. For the wing material, a commercially-available thermosetting resin (Tuffalloy 4282, Hapco, Inc.) was chosen for its ease of use and high Young's modulus (3.2 GPa, as quoted by the manufacturer). This is comparable to the previously reported Young's modulus of the cuticle of insect wings with ranges from 1 to 20 GPa (Smith et al. 2000; Vincent and Wegst 2004; Song et al. 2004, 2007). Details of the fabrication process are described by Tanaka and Wood (2010) with some minor modifications: the bottom mold in the current study has not only corrugations but also veins, resulting in the ability to form veins on both sides of the wing membrane. The cross-sectional shape and sizes of the veins and

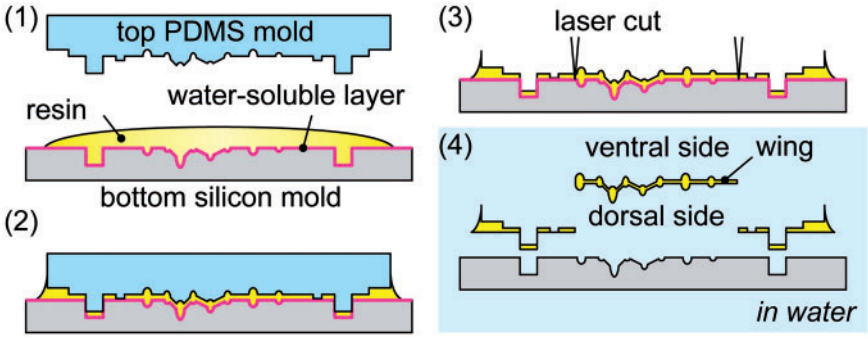

Fig. 3. Schematic representation of the process flow for a corrugated polymer wing. Liquid thermosetting resin was pressed with a pair of molds (1 and 2). After the resin was cured, the top mold was peeled off and a wing outline was cut with a laser (3). Finally the wing was released from the bottom mold in water (4).

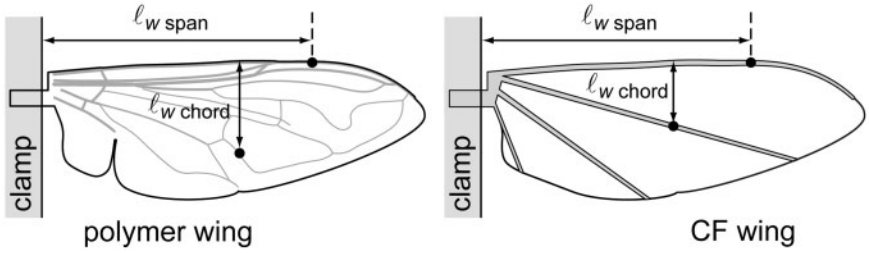

Fig. 4. Locations of the point at which force was applied for flexural stiffness measurements.

corrugations were also modified to achieve stiffness similar to that of the natural wings.

To clarify the effect of wing flexibility, a rigid wing with the same planform shape as the corrugated polymer wing was created (Fig. 2C). The rigid wing consists of an ultra-high-modulus CFRP frame and 1.5 µm-thick polyester film membrane. The CFRP frame was laser-machined from a pre-cured CFRP laminate and bonded to the polyester film with a laser-machined adhesive film. The thickness of the frame was 90 µm, including the adhesive, and the 'vein' width ranges from 75 to 150 µm. The slit at the trailing edge was removed in the rigid wing to avoid fluttering of the membrane. This change of the planform shape increases the wing area and the second moment of wing area around the base only by 0.7% and 0.1%, respectively. It was reported that the mean lift in the quasi-steady analysis is proportional to the second moment of wing area (Weis-Fogh 1973; Ellington 1984a)

The flexibility of both wings were measured by applying a point force to bend the wing in a similar manner as described by Combes and Daniel (2003a). The reduced flexural stiffness EI was approximated from the applied force and the displacement of the wing using simple beam theory, where E is Young's modulus of the beam and I is the second moment of area of the cross section. The setup for the application of a point force to bend the wing was the same as that used by Tanaka and Wood (2010). A point force was applied from the ventral side at approximately 70% of the wing length on the leading edge for spanwise stiffness, and at 70% of the chord width at half the wing length for the chordwise stiffness of the polymer wing (Fig. 4). For the CF wing, the point was adjusted to apply the force to the vein, not the film, in order to prevent damage to the film. The flexural stiffness EI (Nm^2) was calculated as

$$EI = \frac{f l_w^3}{3d}$$

where f is the applied force, l_w is the distance between the applied point force and the proximal mount, and d is the displacement of the wing at the point which force was applied. For chordwise stiffness, we assume that the thick leading edge does not bend.

The torsional stiffness of the artificial wing was controlled by the wing hinge (Fig. 2A). The hinge consists of rigid CFRP sheets and a polyimide film, which was fabricated by a process similar to that used in making the CF wing. The torsional stiffness G (Nm radian^{-1}) can be changed with the hinge width, length, and thickness as

$$G = \frac{E_h w_h t_h^3}{12 l_h}$$

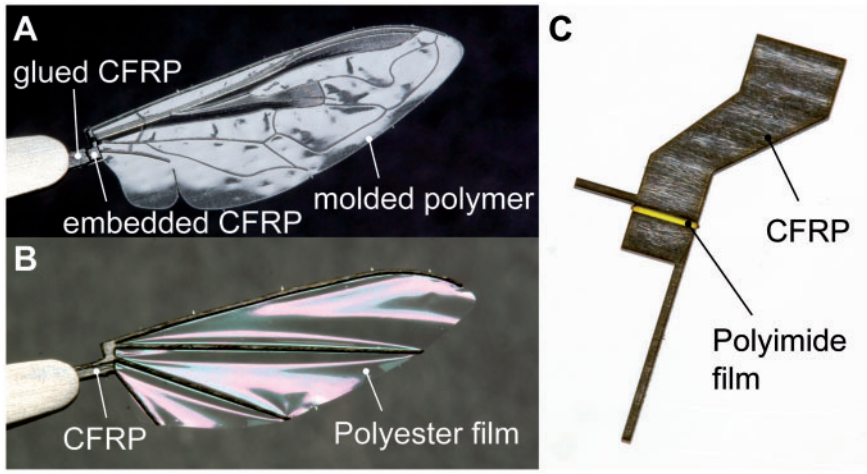

Fig. 5. Photos of a fabricated polymer corrugated wing (**A**) and a rigid carbon-fiber wing (**B**). (**C**) Example of a polyimide flexure hinge. Small lateral and vertical beams were used for motion tracking.

where E_h is Young's modulus of the flexure hinge (2.5 GPa for the polyimide film) and w_h, l_h, t_h are the width, length, and thickness of the hinge, respectively (Fig. 7A). The flexion line of the hinge was set at the root of the thickest vein (Fig. 2A).

At-scale flapping mechanism

Figure 5 shows the fabricated wings and an example hinge. The wings were connected to the flapping mechanism via the wing hinge (Fig. 6). A thermoplastic (Crystalbond 509, Electron Microscopy Sciences) was used for temporary bonding so that the wings and hinges were replaceable. To strengthen the connection between the wing and the wing hinge, a CFRP reinforcement was bonded to the polymer wing with a cyanoacrylate adhesive (Fig. 5A). The tethered flapping mechanism, similar to that used by Whitney and Wood (2010), was driven by a piezoelectric actuator at 150 Hz which is a typical flapping frequency of hovering *E. tenax* (Ellington 1984b; Walker et al. 2009). The sinusoidal input voltage to the piezoelectric actuator was the same in all experiments. The wing motions were captured by two high-speed video cameras (Phantom v7.3, Vision Research) from lateral (front) and vertical (top) perspectives (Fig. 6) using a frame fate of 10,000 fps and an exposure time of 4 µs. Flapping angles, ϕ_b and ϕ_t, are defined by the hinge line and a wing base-tip line in the top view, respectively (Fig. 7B). Φ_h and Φ_t are stroke amplitudes corresponding to ϕ_h and ϕ_t. Wing pitch angles at the base and 75% of the wing length, ψ_b and ψ_w, were measured using a frontal projection view (Fig. 7A and C). Lift was measured using the custom force sensor shown in Fig. 6 at a sampling rate of 10 kHz

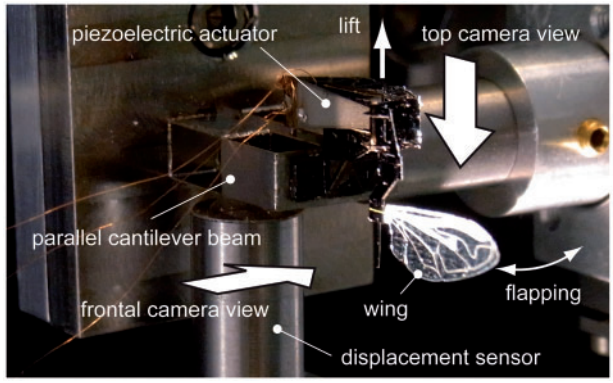

Fig. 6. The tethered flapping mechanism driven by a piezoelectric actuator and flexure-based transmission. Lift was recorded by measuring deflection of a parallel cantilever beam to which the mechanism was attached.

(Wood et al. 2009). The sensor output was filtered *a posteriori* with a cutoff frequency of 750 Hz. Average lift per flapping cycle was calculated as a time-averaged value during 100 flapping cycles. Five measurements were carried out for each combination of wing and hinge.

Our flapping mechanism has only a single wing while a natural hoverfly has a pair of wings that potentially interact both mechanically and aerodynamically. However, in this study, we focus on a single wing, independent of induced flows or disturbances arising from the contralateral wing, the head, thorax, abdomen, or legs.

Results and discussions

Wing flexibility

The measured reduced stiffness, *EI*, and mass of the fabricated wings and a dried specimen of

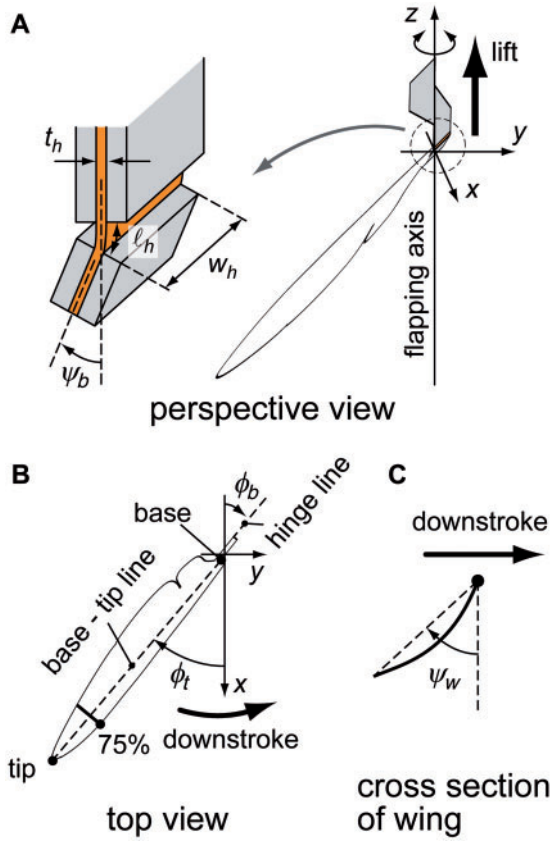

Fig. 7. (**A**) Schematic representation of wing hinge with pitch angle, ψ_b, and perspective view of wing flapping. (**B**) Top view with flapping angle, ϕ. (**C**) Cross-section view of the wing flapping showing wing pitch angle, ψ_w, and chordwise deformation.

E. dimidiata are shown in Table 1. Both spanwise and chordwise stiffness of the corrugated polymer wing achieved the same order of magnitude as those of *E. dimidiata*. On the other hand, the chordwise stiffness of the CF wing was more than three times larger than that of the natural wing. It should be noted that desiccated wing tends to be stiffer and lighter than fresh wing (Steppan 1996; Mengesha 2011). The mass of both polymer and CF wings are approximately equal (~0.9 mg). Since the mass of the artificial wings includes the base attachment, the actual mass of the wing surface should be smaller than the values shown in Table 1.

Five different hinges (very soft, soft, intermediate, rigid, and very rigid) were fabricated with dimensions and calculated stiffnesses quantified in Table 2. Stiffness of the soft and very soft hinges fall between that of *E. tenax* in supination and in pronation.

Wing motion

Observation with a high-speed camera proved that the flexure hinge passively rotated according to the stiffness during tethered flapping. It was also found that the surface of the polymer wing had non-negligible deformation in the chordwise direction, whereas the CF wing behaved as a rigid plate. Figure 8 shows a time sequence of wing pitch angles at the wing base and 75% of the wing length (ψ_b and ψ_w) of the polymer wing and CF wing with an intermediate stiffness hinge. The graphs were smoothed using a nine-point moving-average method to eliminate the error due to manual tracking. For the polymer wing, the magnitude of ψ_w is larger than ψ_b due to the chordwise deformation of the surface (Fig. 8A and C, left). The peak difference of the angles was as large as 30°. In the case of the rigid CF wing, difference between ψ_w and ψ_b was less than 9° (Fig. 8B and C, right).

Table 1. Surface flexural stiffness of artificial and natural wings.

Wing type	Wing length (mm)	Mass (mg)	Spanwise *EI* (Nm^2)	Chordwise *EI* (Nm^2)
polymer	11.7	0.84	3.4×10^{-7}	6.8×10^{-9}
CF (carbon fiber)	11.7	0.88	6.2×10^{-7}	1.7×10^{-8}
sristalis	9.3[a]	0.53[b]	5.4×10^{-7}[a]	4.8×10^{-9}[a]

[a]The values are taken from Tanaka and Wood (2010) for a dried wing of *Eristalis dimidiate*.
[b]The value is taken from Ellington (1984a) for a fresh wing of *Eristalis tenax*.

Figure 9A shows mean values and standard deviations of stroke amplitudes for each combination of the wings and hinges. The flapping amplitude of the wing base, Φ_b, ranged from 82° to 92° and that of the wing tip, Φ_t, ranged from 96° to 112°, respectively. These values for the flapping amplitude of the wing tip are similar to those reported for *E. tenax*, which range from 67° to 131° (Ellington 1984b; Walker et al. 2009). Φ_t tended to be larger than Φ_b. This is due to the offset of the location of the wing tip from the rotational axis of the hinge. Since the offset of the wing tip is larger than that of the base (Fig. 2C), passive pronation at the hinge increased the flapping angle of the wing tip (Fig. 8C) and the supination decreased it, resulting in the greater flapping amplitude of the wing tip. The wing tip flapping amplitude Φ_t of the polymer wing was greater than that of the CF wing despite the fact that the base flapping amplitude Φ_b of the polymer wing was less than that of the CF wing. This is possibly due to the chordwise and spanwise bending of the polymer wing and phase matching between pitch rotation and flapping angles.

Passive pronation and supination was governed by the torsional stiffness of the wing hinge. Figure 9B

Table 2. Torsional stiffness of the wing hinge for the artificial wings and total torsional stiffness measured from natural wings

Hinge type	t_h (μm)	w_h (μm)	l_h (μm)	G (Nm radian^{-1})
Very soft	12.5	1.24×10^3	1.4×10^2	3.5×10^{-6}
Soft	12.5	1.43×10^3	1.3×10^2	4.6×10^{-6}
Intermediate	12.5	1.48×10^3	1.0×10^2	5.9×10^{-6}
Rigid	12.5	1.73×10^3	0.97×10^2	7.2×10^{-6}
Very rigid	12.5	2.07×10^3	1.07×10^2	7.9×10^{-6}
Eristalis (in supination)	–	–	–	1.1×10^{-6}[a]
Eristalis (in pronation)	–	–	–	5.2×10^{-6}[a]

[a]The values are taken from Ennos (1988a) for a fresh wing of *Eristalis tenax*.

shows maximum and minimum wing pitch angles at the wing base ($\psi_{b\max}$ and $\psi_{b\min}$) in pronation (positive value) and supination (negative value). For the polymer wing, $\psi_{b\max}$ and $\psi_{b\min}$ ranged from 13° to 50° and from −18° to −45°, respectively. In the CF wing, $\psi_{b\max}$ and $\psi_{b\min}$ ranged from 23° to 78° and from −25° to −71°, respectively. Rotation of the hinge in the polymer wing was smaller than that of the CF wing across all values of hinge stiffness. This is thought to be due to the chordwise deformation of the surface of the polymer wing. Chordwise deformation reduces the angle of attack of the wing, which presumably decreases drag resulting in reduction of the torque around the wing hinge axis.

The measured average lift is shown in Fig. 9C. A maximum average lift of 6.9×10^2 μN was achieved by the CF wing with a soft hinge (4.6×10^{-6} Nm radian^{-1}). The maximum lift generated by the polymer wing was 5.9×10^2 μN, recorded with the soft hinge. Both wings generated reduced lift with very soft (3.5×10^{-6} Nm radian^{-1}) and very hard (7.9×10^{-6} Nm radian^{-1}) wing hinges, indicating the presence of a (at least local) maximum in lift generation as a function of wing hinge stiffness. Between the soft hinge (4.6×10^{-6} Nm radian^{-1}) and the hard hinge (7.2×10^{-6} Nm radian^{-1}), mean values of average lift were relatively constant: 5.9×10^2 μN for the polymer wing, and ranging from 6.6×10^2 to 6.9×10^2 μN for the CF wing. Given a typical mass of *E. tenax* of 110 mg (Ellington 1984a; Walker et al. 2009), the magnitude of lift produced in these experiments is appropriate for hovering flight. Within this range of torsional stiffness for the greatest lift (4.6×10^{-6} to 7.2×10^{-6} Nm radian^{-1}), the pitching magnitude at the wing base was between 20° and 33° for the polymer wing, and between 28° and 51° for the CF wing (Fig. 9B), which indicates that the compliant surface of the wing causes the passive rotation of the wing hinge to be less sensitive to the torsional compliance at the joint. The range of torsional stiffness which exhibited the greatest lift in the current experiment (4.6×10^{-6} to 7.2×10^{-6} Nm radian^{-1}) overlaps the torsional stiffness of a similarly sized *E. tenax* wing, as measured by Ennos (1988a), which ranges from 1.1×10^{-6} to 5.2×10^{-6} Nm radian^{-1}. It should be noted that Ennos's results include not only torsion at the wing joint but also torsion of the wing surface to some extent due to them method of measurement. Therefore, the actual torsional stiffness at the wing joint of a hoverfly may be larger than the values used in this article.

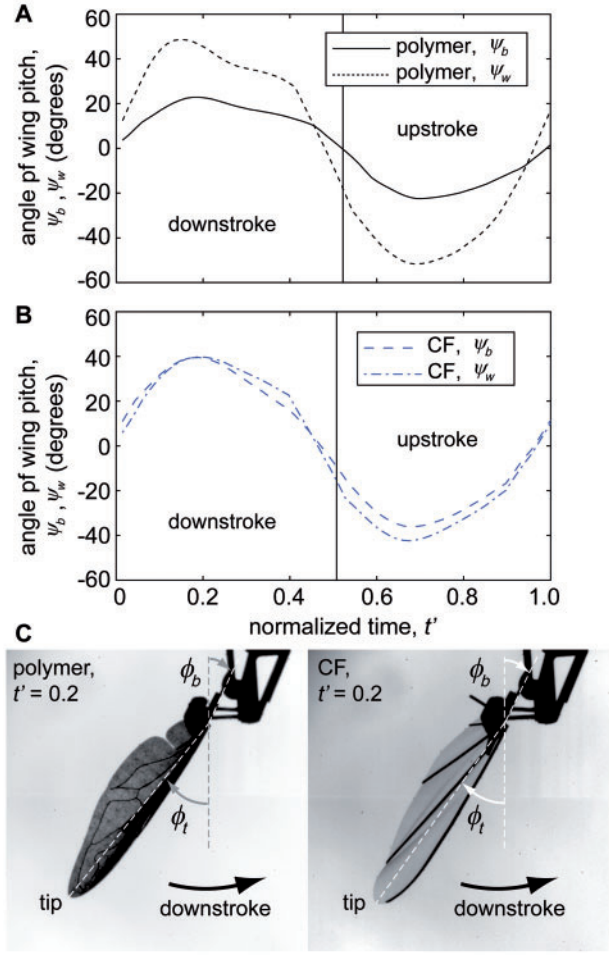

Fig. 8. Time sequence of wing pitch angles at the base and 75% of the wing's length, ψ_b and ψ_w, of a polymer wing (**A**) and CF wing (**B**) with an intermediate hinge. *t'* is a dimensionless time which was normalized by duration of a single flapping cycle. Timing of stroke reversal was determined as the time when the sign of angular velocity of the flapping angle at the base, ϕ_b, changes. (**C**) Top view of the polymer wing (left) and CF wing (right) with the intermediate hinge at $t' = 0.2$. See also Supplementary movies.

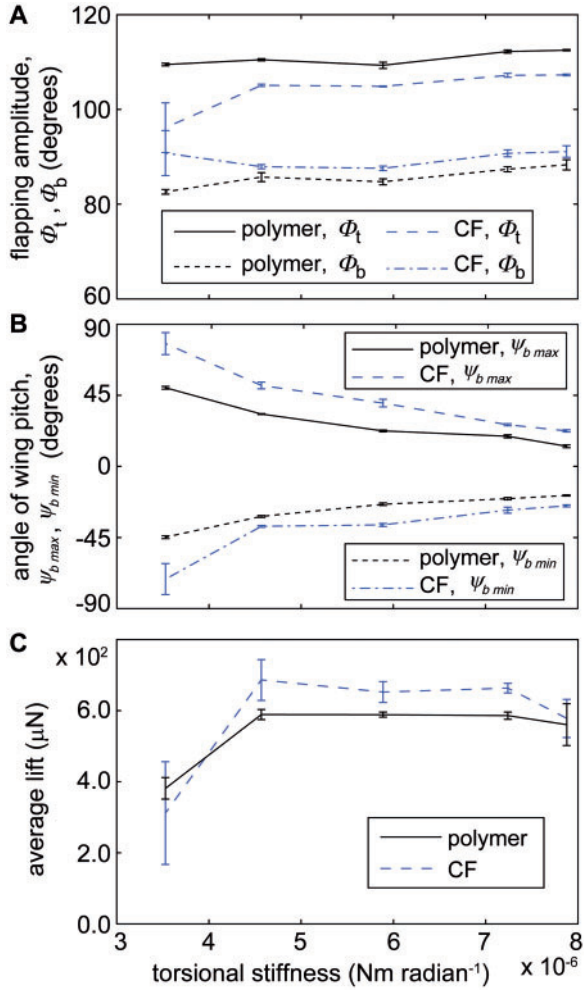

Fig. 9. (**A**) Flapping amplitude of the wing base and the wing tip, Φ_b and Φ_t. (**B**) Maximum and minimum angle of wing pitch at the wing base, $\psi_{b\ max}$ and $\psi_{b\ min}$. (**C**) Average lift per flapping cycle. Flapping frequency was 150 Hz in all cases. Line plots and bars show mean values and standard deviations for five trials.

The current experiments confirm that sufficient lift for hovering can be achieved with passive pronation and supination when the torsional stiffness of the wing joint is similar to that of a natural wing. However, the more rigid CF wing generated on average higher lift than the polymer wing which mimics the flexibility of a natural wing. This suggests that a rigid wing could be more suitable for high lift generation than a flexible wing. However, these experiments do not consider input power (either electrical power to the actuator or mechanical power to the wing transmission) and only use lift as a metric for performance. To more fully understand the effect of wing flexibility for flapping-wing flight, the drag force and efficiency also need to be investigated. Furthermore, the polymer wing used in these experiments was not optimized for generation or efficiency of thrust; it is reasonable to expect that performance would be improved by appropriate choice of design (biomimetic or otherwise). For example, negative camber appeared in our current polymer wing during flapping, whereas positive camber was reported in natural wings during free flight (Walker et al. 2009).

Conclusion

To evaluate the effect of flexural and torsional compliance on lift generation in dipteran flight, a flexible polymer wing and multiple compliant hinge joints were created to have similar dimensions as natural hoverfly wings. The polymer wing mimicked the venation and surface corrugations of a hoverfly, *E. tenax*, at the scale of the insect. The 3D veins and membranes were formed simultaneously by a single molding process using laser-machined micromolds. Measured spanwise and chordwise stiffnesses *EI* were $3.4 \times 10^{-7}\,\mathrm{Nm}^2$ and $6.8 \times 10^{-9}\,\mathrm{Nm}^2$, respectively, which were the same order of magnitude as those of a dried *E. dimidiata*. A single flexure hinge was used to control the torsional flexibility of the joint connecting the wing and the body. The artificial wings and hinges were tested with an at-scale tethered flapping mechanism driven by a piezoelectric actuator. It was found that the flexure hinge passively pronated and supinated during tethered flapping when the stiffness of the hinge was similar to the torsional stiffness of fresh *Eristalis tenax* wings. By comparing the flexible polymer wing with a rigid carbon-fiber (CF) wing, it was found that the rotation of the wing hinge for the polymer wing was less than that for the CF wing, which is thought to be due to chordwise deformation of the polymer wing. When the stiffness of the hinge was between 4.6×10^{-6} and $7.2 \times 10^{-6}\,\mathrm{Nm\ radian}^{-1}$, both the polymer and the CF wing produced sufficiently large lift for a hovering *Eristalis*. The maximum lift achieved with the CF wing, $6.9 \times 10^2\,\mu\mathrm{N}$, was greater than that of the polymer wing, $5.9 \times 10^2\,\mu\mathrm{N}$. These results suggest that hoverflies can utilize passively pronation and supination during hovering flight, and that for similar wing flapping motions and wing planforms, a rigid wing can produce larger lift. The effect of wing flexibility on drag and efficiency, however, require further investigation.

Finally, a key demonstration of this work is that the use of at-scale test apparatus—including biomimetic wings, flapping mechanism, and associated instrumentation—provides unprecedented capabilities for the study of structure–function relationships for insect-like flapping wings. Such experiments

require no scaling assumptions and can use a large variety of artificial wings or freshly excised insect wings.

Acknowledgments

The authors acknowledge support of the Wyss Institute for Biologically Inspired Engineering and the facilities in the Harvard Center for Nanoscale Systems.

Funding

This work was supported by the National Science Foundation (award number CCF-0926148) and the Air Force Office of Scientific Research (award number FA9550-09-1-0156). Any opinions, findings, and conclusions or recommendations expressed in this material are those of the author and do not necessarily reflect the views of the National Science Foundation.

Supplementary Data

Supplementary Data are available at *ICB* online.

References

Birch JM, Dickinson MH. 2001. Spanwise flow and the attachment of the leading-edge vortex on insect wings. Nature 412:729–33.

Brodsky AK. 1994. The evolution of insect flight. New York: Oxford University Press.

Combes SA, Daniel TL. 2003a. Flexural stiffness in insect wings I. Scaling and the influence of wing venation. J Exp Biol 206:2979–87.

Combes SA, Daniel TL. 2003b. Into thin air: contributions of aerodynamic and inertial-elastic forces to wing bending in the hawkmoth Manduca sexta. J Exp Biol 206:2999–3006.

Dickinson MH, Lehmann FO, Sane SP. 1999. Wing rotation and the aerodynamic basis of insect flight. Science 284:1954–60.

Ellington CP. 1984a. The aerodynamics of hovering insect flight II. Morphological parameters. Phil Trans Roy Soc Lond B Biol Sci 305:17–40.

Ellington CP. 1984b. The aerodynamics of hovering insect flight III. Kinematics. Phil Trans Roy Soc Lond B Biol Sci 305:41–78.

Ennos AR. 1988a. The importance of torsion in the design of insect wings. J Exp Biol 140:137–60.

Ennos AR. 1988b. The inertial cause of wing totation in Diptera. J Exp Biol 140:161–9.

Fry SN, Sayaman R, Dickinson MH. 2003. The aerodynamics of free-flight maneuvers in Drosophila. Science 300:495–8.

Ishihara D, Yamashita Y, Horie T, Yoshida S, Niho T. 2009. Passive maintenance of high angle of attack and its lift generation during flapping translation in crane fly wing. J Exp Biol 212:3882–91.

Jongerius S, Lentink D. 2010. Structural analysis of a dragonfly wing. Exp Mech 50:1323–34.

Mengesha TE, Vallance RR, Mittal R. 2011. Stiffness of desiccating insect wings. Bioinsp Biomim 6:014001.

Okamoto M, Yasuda K, Azuma A. 1996. Aerodynamic characteristics of the wings and body of a dragonfly. J Exp Biol 199:281–94.

Rees CJC. 1975. Form and function in corrugated insect wings. Nature 256:200–3.

Sane SP. 2003. The aerodynamics of insect flight. J Exp Biol 206:4191–208.

Smith CW, Herbert R, Wootton RJ, Evans KE. 2000. The hind wing of the desert locust (Schistocerca gregaria Forskal) II. Mechanical properties and functioning of the membrane. J Exp Biol 203:2933–43.

Song F, Lee KL, Soh AK, Zhu F, Bai YL. 2004. Experimental studies of the material properties of the forewing of cicada (Homoptera, Cicadidae). J Exp Biol 207:3035–42.

Song F, Xiao KW, Bai K, Bai YL. 2007. Microstructure and nanomechanical properties of the wing membrane of dragonfly. Mater Sci Eng A-Struct Mater Prop Microstruct Process 457:254–60.

Steppan SJ. 1996. Flexural stiffness patterns of butterfly wings (Papilionoidea). Journal of Research on the Lepidoptera. 35:61–77.

Tanaka H, Wood RJ. 2010. Fabrication of corrugated artificial insect wings using laser micromachined molds. J Micromech Microeng 20:075008.

Vincent JFV, Wegst UGK. 2004. Design and mechanical properties of insect cuticle. Arthropod Struct Dev 33:187–99.

Walker SM, Thomas ALR, Taylor GK. 2010. Deformable wing kinematics in free-flying hoverflies. J Roy Soc Interface 7:131–42.

Weis-Fogh T. 1973. Quick estimates of flight fitness in hovering animals, including novel mechanisms for lift production. J Exp Biol 59:169–230.

Whitney JP, Wood RJ. 2010. Aeromechanics of passive rotation in flapping flight. J Fluid Mech 660:197–220.

Wood RJ, Cho KJ, Hoffman K. 2009. A novel multi-axis force sensor for microrobotics applications. Smart Mater Struct 18:125002.

Wood RJ. 2008. The first takeoff of a biologically inspired at-scale robotic insect. IEEE Trans Robotics 24:341–7.

Wootton RJ. 1992. Functional-morphology of insect wings. Annu Rev Entomol 37:113–40.

Zhao L, Huang QF, Deng XY, Sane SP. 2010. Aerodynamic effects of flexibility in flapping wings. J Roy Soc Interface 7:485–97.